Determination of the form factors for the decay $B^0 \to D^{*-} l^+ \nu_l$ and of the CKM matrix element $|V_{cb}|$

B. Aubert,[1] M. Bona,[1] D. Boutigny,[1] Y. Karyotakis,[1] J. P. Lees,[1] V. Poireau,[1] X. Prudent,[1] V. Tisserand,[1] A. Zghiche,[1] J. Garra Tico,[2] E. Grauges,[2] L. Lopez,[3] A. Palano,[3] G. Eigen,[4] I. Ofte,[4] B. Stugu,[4] L. Sun,[4] G. S. Abrams,[5] M. Battaglia,[5] D. N. Brown,[5] J. Button-Shafer,[5] R. N. Cahn,[5] Y. Groysman,[5] R. G. Jacobsen,[5] J. A. Kadyk,[5] L. T. Kerth,[5] Yu. G. Kolomensky,[5] G. Kukartsev,[5] D. Lopes Pegna,[5] G. Lynch,[5] L. M. Mir,[5] T. J. Orimoto,[5] M. Pripstein,[5] N. A. Roe,[5] M. T. Ronan,[5,*] K. Tackmann,[5] W. A. Wenzel,[5] P. del Amo Sanchez,[6] C. M. Hawkes,[6] A. T. Watson,[6] T. Held,[7] H. Koch,[7] B. Lewandowski,[7] M. Pelizaeus,[7] T. Schroeder,[7] M. Steinke,[7] W. N. Cottingham,[8] D. Walker,[8] D. J. Asgeirsson,[9] T. Cuhadar-Donszelmann,[9] B. G. Fulsom,[9] C. Hearty,[9] N. S. Knecht,[9] T. S. Mattison,[9] J. A. McKenna,[9] A. Khan,[10] M. Saleem,[10] L. Teodorescu,[10] V. E. Blinov,[11] A. D. Bukin,[11] V. P. Druzhinin,[11] V. B. Golubev,[11] A. P. Onuchin,[11] S. I. Serednyakov,[11] Yu. I. Skovpen,[11] E. P. Solodov,[11] K. Yu Todyshev,[11] M. Bondioli,[12] S. Curry,[12] I. Eschrich,[12] D. Kirkby,[12] A. J. Lankford,[12] P. Lund,[12] M. Mandelkern,[12] E. C. Martin,[12] D. P. Stoker,[12] S. Abachi,[13] C. Buchanan,[13] S. D. Foulkes,[14] J. W. Gary,[14] F. Liu,[14] O. Long,[14] B. C. Shen,[14] L. Zhang,[14] H. P. Paar,[15] S. Rahatlou,[15] V. Sharma,[15] J. W. Berryhill,[16] C. Campagnari,[16] A. Cunha,[16] B. Dahmes,[16] T. M. Hong,[16] D. Kovalskyi,[16] J. D. Richman,[16] T. W. Beck,[17] A. M. Eisner,[17] C. J. Flacco,[17] C. A. Heusch,[17] J. Kroseberg,[17] W. S. Lockman,[17] T. Schalk,[17] B. A. Schumm,[17] A. Seiden,[17] D. C. Williams,[17] M. G. Wilson,[17] L. O. Winstrom,[17] E. Chen,[18] C. H. Cheng,[18] A. Dvoretskii,[18] F. Fang,[18] D. G. Hitlin,[18] I. Narsky,[18] T. Piatenko,[18] F. C. Porter,[18] G. Mancinelli,[19] B. T. Meadows,[19] K. Mishra,[19] M. D. Sokoloff,[19] F. Blanc,[20] P. C. Bloom,[20] S. Chen,[20] W. T. Ford,[20] J. F. Hirschauer,[20] A. Kreisel,[20] M. Nagel,[20] U. Nauenberg,[20] A. Olivas,[20] J. G. Smith,[20] K. A. Ulmer,[20] S. R. Wagner,[20] J. Zhang,[20] A. M. Gabareen,[21] A. Soffer,[21] W. H. Toki,[21] R. J. Wilson,[21] F. Winklmeier,[21] Q. Zeng,[21] D. D. Altenburg,[22] E. Feltresi,[22] A. Hauke,[22] H. Jasper,[22] J. Merkel,[22] A. Petzold,[22] B. Spaan,[22] K. Wacker,[22] T. Brandt,[23] V. Klose,[23] H. M. Lacker,[23] W. F. Mader,[23] R. Nogowski,[23] J. Schubert,[23] K. R. Schubert,[23] R. Schwierz,[23] J. E. Sundermann,[23] A. Volk,[23] D. Bernard,[24] G. R. Bonneaud,[24] E. Latour,[24] V. Lombardo,[24] Ch. Thiebaux,[24] M. Verderi,[24] P. J. Clark,[25] W. Gradl,[25] F. Muheim,[25] S. Playfer,[25] A. I. Robertson,[25] Y. Xie,[25] M. Andreotti,[26] D. Bettoni,[26] C. Bozzi,[26] R. Calabrese,[26] A. Cecchi,[26] G. Cibinetto,[26] P. Franchini,[26] E. Luppi,[26] M. Negrini,[26] A. Petrella,[26] L. Piemontese,[26] E. Prencipe,[26] V. Santoro,[26] F. Anulli,[27] R. Baldini-Ferroli,[27] A. Calcaterra,[27] R. de Sangro,[27] G. Finocchiaro,[27] S. Pacetti,[27] P. Patteri,[27] I. M. Peruzzi,[27,†] M. Piccolo,[27] M. Rama,[27] A. Zallo,[27] A. Buzzo,[28] R. Contri,[28] M. Lo Vetere,[28] M. M. Macri,[28] M. R. Monge,[28] S. Passaggio,[28] C. Patrignani,[28] E. Robutti,[28] A. Santroni,[28] S. Tosi,[28] K. S. Chaisanguanthum,[29] M. Morii,[29] J. Wu,[29] R. S. Dubitzky,[30] J. Marks,[30] S. Schenk,[30] U. Uwer,[30] D. J. Bard,[31] P. D. Dauncey,[31] R. L. Flack,[31] J. A. Nash,[31] M. B. Nikolich,[31] W. Panduro Vazquez,[31] P. K. Behera,[32] X. Chai,[32] M. J. Charles,[32] U. Mallik,[32] N. T. Meyer,[32] V. Ziegler,[32] J. Cochran,[33] H. B. Crawley,[33] L. Dong,[33] V. Eyges,[33] W. T. Meyer,[33] S. Prell,[33] E. I. Rosenberg,[33] A. E. Rubin,[33] A. V. Gritsan,[34] Z. J. Guo,[34] C. K. Lae,[34] A. G. Denig,[35] M. Fritsch,[35] G. Schott,[35] N. Arnaud,[36] J. Béquilleux,[36] M. Davier,[36] G. Grosdidier,[36] A. Höcker,[36] V. Lepeltier,[36] F. Le Diberder,[36] A. M. Lutz,[36] S. Pruvot,[36] S. Rodier,[36] P. Roudeau,[36] M. H. Schune,[36] J. Serrano,[36] V. Sordini,[36] A. Stocchi,[36] W. F. Wang,[36] G. Wormser,[36] D. J. Lange,[37] D. M. Wright,[37] C. A. Chavez,[38] I. J. Forster,[38] J. R. Fry,[38] E. Gabathuler,[38] R. Gamet,[38] D. E. Hutchcroft,[38] D. J. Payne,[38] K. C. Schofield,[38] C. Touramanis,[38] A. J. Bevan,[39] F. Di Lodovico,[39] K. A. George,[39] W. Menges,[39] R. Sacco,[39] G. Cowan,[40] H. U. Flaecher,[40] D. A. Hopkins,[40] P. S. Jackson,[40] T. R. McMahon,[40] F. Salvatore,[40] A. C. Wren,[40] D. N. Brown,[41] C. L. Davis,[41] J. Allison,[42] N. R. Barlow,[42] R. J. Barlow,[42] Y. M. Chia,[42] C. L. Edgar,[42] G. D. Lafferty,[42] T. J. West,[42] J. I. Yi,[42] J. Anderson,[43] C. Chen,[43] A. Jawahery,[43] D. A. Roberts,[43] G. Simi,[43] J. M. Tuggle,[43] G. Blaylock,[44] C. Dallapiccola,[44] S. S. Hertzbach,[44] X. Li,[44] T. B. Moore,[44] E. Salvati,[44] S. Saremi,[44] R. Cowan,[45] P. H. Fisher,[45] G. Sciolla,[45] S. J. Sekula,[45] M. Spitznagel,[45] F. Taylor,[45] R. K. Yamamoto,[45] S. E. Mclachlin,[46] P. M. Patel,[46] S. H. Robertson,[46] A. Lazzaro,[47] F. Palombo,[47] J. M. Bauer,[48] L. Cremaldi,[48] V. Eschenburg,[48] R. Godang,[48] R. Kroeger,[48] D. A. Sanders,[48] D. J. Summers,[48] H. W. Zhao,[48] S. Brunet,[49] D. Côté,[49] M. Simard,[49] P. Taras,[49] F. B. Viaud,[49] H. Nicholson,[50] G. De Nardo,[51] F. Fabozzi,[51,‡] L. Lista,[51] D. Monorchio,[51] C. Sciacca,[51] M. A. Baak,[52] G. Raven,[52] H. L. Snoek,[52] C. P. Jessop,[53] J. M. LoSecco,[53] G. Benelli,[54] L. A. Corwin,[54] K. K. Gan,[54] K. Honscheid,[54] D. Hufnagel,[54] H. Kagan,[54] R. Kass,[54] J. P. Morris,[54] A. M. Rahimi,[54] J. J. Regensburger,[54] R. Ter-Antonyan,[54] Q. K. Wong,[54] N. L. Blount,[55] J. Brau,[55] R. Frey,[55] O. Igonkina,[55] J. A. Kolb,[55] M. Lu,[55] R. Rahmat,[55] N. B. Sinev,[55] D. Strom,[55] J. Strube,[55] E. Torrence,[55] N. Gagliardi,[56] A. Gaz,[56] M. Margoni,[56] M. Morandin,[56] A. Pompili,[56] M. Posocco,[56] M. Rotondo,[56] F. Simonetto,[56] R. Stroili,[56] C. Voci,[56] E. Ben-Haim,[57] H. Briand,[57] J. Chauveau,[57] P. David,[57] L. Del Buono,[57] Ch. de la Vaissière,[57] O. Hamon,[57] B. L. Hartfiel,[57] Ph. Leruste,[57] J. Malclès,[57] J. Ocariz,[57]

A. Perez,[57] L. Gladney,[58] M. Biasini,[59] R. Covarelli,[59] E. Manoni,[59] C. Angelini,[60] G. Batignani,[60] S. Bettarini,[60] G. Calderini,[60] M. Carpinelli,[60] R. Cenci,[60] A. Cervelli,[60] F. Forti,[60] M. A. Giorgi,[60] A. Lusiani,[60] G. Marchiori,[60] M. A. Mazur,[60] M. Morganti,[60] N. Neri,[60] E. Paoloni,[60] G. Rizzo,[60] J. J. Walsh,[60] M. Haire,[61] J. Biesiada,[62] P. Elmer,[62] Y. P. Lau,[62] C. Lu,[62] J. Olsen,[62] A. J. S. Smith,[62] A. V. Telnov,[62] E. Baracchini,[63] F. Bellini,[63] G. Cavoto,[63] A. D'Orazio,[63] D. del Re,[63] E. Di Marco,[63] R. Faccini,[63] F. Ferrarotto,[63] F. Ferroni,[63] M. Gaspero,[63] P. D. Jackson,[63] L. Li Gioi,[63] M. A. Mazzoni,[63] S. Morganti,[63] G. Piredda,[63] F. Polci,[63] F. Renga,[63] C. Voena,[63] M. Ebert,[64] H. Schröder,[64] R. Waldi,[64] T. Adye,[65] G. Castelli,[65] B. Franek,[65] E. O. Olaiya,[65] S. Ricciardi,[65] W. Roethel,[65] F. F. Wilson,[65] R. Aleksan,[66] S. Emery,[66] M. Escalier,[66] A. Gaidot,[66] S. F. Ganzhur,[66] G. Hamel de Monchenault,[66] W. Kozanecki,[66] M. Legendre,[66] G. Vasseur,[66] Ch. Yèche,[66] M. Zito,[66] X. R. Chen,[67] H. Liu,[67] W. Park,[67] M. V. Purohit,[67] J. R. Wilson,[67] M. T. Allen,[68] D. Aston,[68] R. Bartoldus,[68] P. Bechtle,[68] N. Berger,[68] R. Claus,[68] J. P. Coleman,[68] M. R. Convery,[68] J. C. Dingfelder,[68] J. Dorfan,[68] G. P. Dubois-Felsmann,[68] D. Dujmic,[68] W. Dunwoodie,[68] R. C. Field,[68] T. Glanzman,[68] S. J. Gowdy,[68] M. T. Graham,[68] P. Grenier,[68] C. Hast,[68] T. Hryn'ova,[68] W. R. Innes,[68] M. H. Kelsey,[68] H. Kim,[68] P. Kim,[68] D. W. G. S. Leith,[68] S. Li,[68] S. Luitz,[68] V. Luth,[68] H. L. Lynch,[68] D. B. MacFarlane,[68] H. Marsiske,[68] R. Messner,[68] D. R. Muller,[68] C. P. O'Grady,[68] A. Perazzo,[68] M. Perl,[68] T. Pulliam,[68] B. N. Ratcliff,[68] A. Roodman,[68] A. A. Salnikov,[68] R. H. Schindler,[68] J. Schwiening,[68] A. Snyder,[68] J. Stelzer,[68] D. Su,[68] M. K. Sullivan,[68] K. Suzuki,[68] S. K. Swain,[68] J. M. Thompson,[68] J. Va'vra,[68] N. van Bakel,[68] A. P. Wagner,[68] M. Weaver,[68] W. J. Wisniewski,[68] M. Wittgen,[68] D. H. Wright,[68] A. K. Yarritu,[68] K. Yi,[68] C. C. Young,[68] P. R. Burchat,[69] A. J. Edwards,[69] S. A. Majewski,[69] B. A. Petersen,[69] L. Wilden,[69] S. Ahmed,[70] M. S. Alam,[70] R. Bula,[70] J. A. Ernst,[70] V. Jain,[70] B. Pan,[70] M. A. Saeed,[70] F. R. Wappler,[70] S. B. Zain,[70] W. Bugg,[71] M. Krishnamurthy,[71] S. M. Spanier,[71] R. Eckmann,[72] J. L. Ritchie,[72] A. M. Ruland,[72] C. J. Schilling,[72] R. F. Schwitters,[72] J. M. Izen,[73] X. C. Lou,[73] S. Ye,[73] F. Bianchi,[74] F. Gallo,[74] D. Gamba,[74] M. Pelliccioni,[74] M. Bomben,[75] L. Bosisio,[75] C. Cartaro,[75] F. Cossutti,[75] G. Della Ricca,[75] L. Lanceri,[75] L. Vitale,[75] V. Azzolini,[76] N. Lopez-March,[76] F. Martinez-Vidal,[76] D. A. Milanes,[76] A. Oyanguren,[76] J. Albert,[77] Sw. Banerjee,[77] B. Bhuyan,[77] K. Hamano,[77] R. Kowalewski,[77] I. M. Nugent,[77] J. M. Roney,[77] R. J. Sobie,[77] J. J. Back,[78] P. F. Harrison,[78] T. E. Latham,[78] G. B. Mohanty,[78] M. Pappagallo,[78,§] H. R. Band,[79] X. Chen,[79] S. Dasu,[79] K. T. Flood,[79] J. J. Hollar,[79] P. E. Kutter,[79] Y. Pan,[79] M. Pierini,[79] R. Prepost,[79] S. L. Wu,[79] Z. Yu,[79] and H. Neal[80]

(*BABAR* Collaboration)

[1]*Laboratoire de Physique des Particules, IN2P3/CNRS et Université de Savoie, F-74941 Annecy-Le-Vieux, France*
[2]*Universitat de Barcelona, Facultat de Fisica, Departament ECM, E-08028 Barcelona, Spain*
[3]*Università di Bari, Dipartimento di Fisica and INFN, I-70126 Bari, Italy*
[4]*University of Bergen, Institute of Physics, N-5007 Bergen, Norway*
[5]*Lawrence Berkeley National Laboratory and University of California, Berkeley, California 94720, USA*
[6]*University of Birmingham, Birmingham, B15 2TT, United Kingdom*
[7]*Ruhr Universität Bochum, Institut für Experimentalphysik 1, D-44780 Bochum, Germany*
[8]*University of Bristol, Bristol BS8 1TL, United Kingdom*
[9]*University of British Columbia, Vancouver, British Columbia, Canada V6T 1Z1*
[10]*Brunel University, Uxbridge, Middlesex UB8 3PH, United Kingdom*
[11]*Budker Institute of Nuclear Physics, Novosibirsk 630090, Russia*
[12]*University of California at Irvine, Irvine, California 92697, USA*
[13]*University of California at Los Angeles, Los Angeles, California 90024, USA*
[14]*University of California at Riverside, Riverside, California 92521, USA*
[15]*University of California at San Diego, La Jolla, California 92093, USA*
[16]*University of California at Santa Barbara, Santa Barbara, California 93106, USA*
[17]*University of California at Santa Cruz, Institute for Particle Physics, Santa Cruz, California 95064, USA*
[18]*California Institute of Technology, Pasadena, California 91125, USA*
[19]*University of Cincinnati, Cincinnati, Ohio 45221, USA*
[20]*University of Colorado, Boulder, Colorado 80309, USA*
[21]*Colorado State University, Fort Collins, Colorado 80523, USA*
[22]*Universität Dortmund, Institut für Physik, D-44221 Dortmund, Germany*
[23]*Technische Universität Dresden, Institut für Kern- und Teilchenphysik, D-01062 Dresden, Germany*
[24]*Laboratoire Leprince-Ringuet, CNRS/IN2P3, Ecole Polytechnique, F-91128 Palaiseau, France*
[25]*University of Edinburgh, Edinburgh EH9 3JZ, United Kingdom*
[26]*Università di Ferrara, Dipartimento di Fisica and INFN, I-44100 Ferrara, Italy*
[27]*Laboratori Nazionali di Frascati dell'INFN, I-00044 Frascati, Italy*

[28]*Università di Genova, Dipartimento di Fisica and INFN, I-16146 Genova, Italy*
[29]*Harvard University, Cambridge, Massachusetts 02138, USA*
[30]*Universität Heidelberg, Physikalisches Institut, Philosophenweg 12, D-69120 Heidelberg, Germany*
[31]*Imperial College London, London, SW7 2AZ, United Kingdom*
[32]*University of Iowa, Iowa City, Iowa 52242, USA*
[33]*Iowa State University, Ames, Iowa 50011-3160, USA*
[34]*Johns Hopkins University, Baltimore, Maryland 21218, USA*
[35]*Universität Karlsruhe, Institut für Experimentelle Kernphysik, D-76021 Karlsruhe, Germany*
[36]*Laboratoire de l'Accélérateur Linéaire, IN2P3/CNRS et Université Paris-Sud 11, Centre Scientifique d'Orsay, B. P. 34, F-91898 ORSAY Cedex, France*
[37]*Lawrence Livermore National Laboratory, Livermore, California 94550, USA*
[38]*University of Liverpool, Liverpool L69 7ZE, United Kingdom*
[39]*Queen Mary, University of London, E1 4NS, United Kingdom*
[40]*University of London, Royal Holloway and Bedford New College, Egham, Surrey TW20 0EX, United Kingdom*
[41]*University of Louisville, Louisville, Kentucky 40292, USA*
[42]*University of Manchester, Manchester M13 9PL, United Kingdom*
[43]*University of Maryland, College Park, Maryland 20742, USA*
[44]*University of Massachusetts, Amherst, Massachusetts 01003, USA*
[45]*Massachusetts Institute of Technology, Laboratory for Nuclear Science, Cambridge, Massachusetts 02139, USA*
[46]*McGill University, Montréal, Québec, Canada H3A 2T8*
[47]*Università di Milano, Dipartimento di Fisica and INFN, I-20133 Milano, Italy*
[48]*University of Mississippi, University, Mississippi 38677, USA*
[49]*Université de Montréal, Physique des Particules, Montréal, Québec, Canada H3C 3J7*
[50]*Mount Holyoke College, South Hadley, Massachusetts 01075, USA*
[51]*Università di Napoli Federico II, Dipartimento di Scienze Fisiche and INFN, I-80126, Napoli, Italy*
[52]*NIKHEF, National Institute for Nuclear Physics and High Energy Physics, NL-1009 DB Amsterdam, The Netherlands*
[53]*University of Notre Dame, Notre Dame, Indiana 46556, USA*
[54]*Ohio State University, Columbus, Ohio 43210, USA*
[55]*University of Oregon, Eugene, Oregon 97403, USA*
[56]*Università di Padova, Dipartimento di Fisica and INFN, I-35131 Padova, Italy*
[57]*Laboratoire de Physique Nucléaire et de Hautes Energies, IN2P3/CNRS, Université Pierre et Marie Curie-Paris6, Université Denis Diderot-Paris7, F-75252 Paris, France*
[58]*University of Pennsylvania, Philadelphia, Pennsylvania 19104, USA*
[59]*Università di Perugia, Dipartimento di Fisica and INFN, I-06100 Perugia, Italy*
[60]*Università di Pisa, Dipartimento di Fisica, Scuola Normale Superiore and INFN, I-56127 Pisa, Italy*
[61]*Prairie View A&M University, Prairie View, Texas 77446, USA*
[62]*Princeton University, Princeton, New Jersey 08544, USA*
[63]*Università di Roma La Sapienza, Dipartimento di Fisica and INFN, I-00185 Roma, Italy*
[64]*Universität Rostock, D-18051 Rostock, Germany*
[65]*Rutherford Appleton Laboratory, Chilton, Didcot, Oxon, OX11 0QX, United Kingdom*
[66]*DSM/Dapnia, CEA/Saclay, F-91191 Gif-sur-Yvette, France*
[67]*University of South Carolina, Columbia, South Carolina 29208, USA*
[68]*Stanford Linear Accelerator Center, Stanford, California 94309, USA*
[69]*Stanford University, Stanford, California 94305-4060, USA*
[70]*State University of New York, Albany, New York 12222, USA*
[71]*University of Tennessee, Knoxville, Tennessee 37996, USA*
[72]*University of Texas at Austin, Austin, Texas 78712, USA*
[73]*University of Texas at Dallas, Richardson, Texas 75083, USA*
[74]*Università di Torino, Dipartimento di Fisica Sperimentale and INFN, I-10125 Torino, Italy*
[75]*Università di Trieste, Dipartimento di Fisica and INFN, I-34127 Trieste, Italy*
[76]*IFIC, Universitat de Valencia-CSIC, E-46071 Valencia, Spain*
[77]*University of Victoria, Victoria, British Columbia, Canada V8W 3P6*
[78]*Department of Physics, University of Warwick, Coventry CV4 7AL, United Kingdom*
[79]*University of Wisconsin, Madison, Wisconsin 53706, USA*
[80]*Yale University, New Haven, Connecticut 06511, USA*

[*]Deceased.
[†]Also with Università di Perugia, Dipartimento di Fisica, Perugia, Italy.
[‡]Also with Università della Basilicata, Potenza, Italy.
[§]Also with IPPP, Physics Department, Durham University, Durham DH1 3LE, United Kingdom.

(Received 30 May 2007; published 15 February 2008)

We present a combined measurement of the Cabibbo-Kobayashi-Maskawa matrix element $|V_{cb}|$ and of the parameters ρ^2, $R_1(1)$, and $R_2(1)$, which fully characterize the form factors for the $B^0 \to D^{*-}\ell^+\nu_\ell$ decay in the framework of heavy-quark effective field theory. The results, based on a selected sample of about 52 800 $B^0 \to D^{*-}\ell^+\nu_\ell$ decays, recorded by the *BABAR* detector, are $\rho^2 = 1.157 \pm 0.094 \pm 0.027$, $R_1(1) = 1.327 \pm 0.131 \pm 0.043$, $R_2(1) = 0.859 \pm 0.077 \pm 0.021$, and $\mathcal{F}(1)|V_{cb}| = (34.7 \pm 0.4 \pm 1.0) \times 10^{-3}$. The first error is the statistical and the second is the systematic uncertainty. Combining these measurements with the previous *BABAR* measurement of the form factors, which employs a different fit technique on a partial sample of the data, we improve the statistical precision of the result, $\rho^2 = 1.191 \pm 0.048 \pm 0.028$, $R_1(1) = 1.429 \pm 0.061 \pm 0.044$, $R_2(1) = 0.827 \pm 0.038 \pm 0.022$, and $\mathcal{F}(1)|V_{cb}| = (34.4 \pm 0.3 \pm 1.1) \times 10^{-3}$. Using lattice calculations for the axial form factor $\mathcal{F}(1)$, we extract $|V_{cb}| = (37.4 \pm 0.3 \pm 1.2^{+1.2}_{-1.4}) \times 10^{-3}$, where the third error is due to the uncertainty in $\mathcal{F}(1)$. We also present a measurement of the exclusive branching fraction, $\mathcal{B} = (4.69 \pm 0.04 \pm 0.34)\%$.

DOI: 10.1103/PhysRevD.77.032002 PACS numbers: 13.25.Hw, 12.15.Hh, 11.30.Er

I. INTRODUCTION

The study of the semileptonic decay $B^0 \to D^{*-}\ell^+\nu_\ell$ [1] is interesting in many respects. In the standard model, the rate of this weak decay is proportional to the square of the Cabibbo-Kobayashi-Maskawa (CKM) matrix element V_{cb}, which is a measure of the weak coupling of the b to the c quark. This decay is also influenced by strong interactions. Their effect can be parametrized by two axial form factors, A_1 and A_2, and one vector form factor, V, each of which depends on the momentum transfer squared q^2 of the B meson to the D^* meson. The form of this dependence is not known *a priori*. In the framework of heavy-quark effective field theory (HQET) [2,3], these three form factors are related to each other through heavy-quark symmetry (HQS), but HQET leaves three free parameters, which must be determined by experiment.

The extraction of $|V_{cb}|$ relies on the measurement of differential decay rates. HQS predicts the normalization of the decay rate at the maximum q^2, and $|V_{cb}|$ is determined from an extrapolation of the form factors to this value. The precise determination requires corrections to the HQS prediction for the normalization, as well as a measurement of the variation of the form factors near the maximum q^2, where the decay rate goes to zero as the phase space vanishes.

Several experiments have measured $|V_{cb}|$ based on studies of the differential decay width for $B^0 \to D^{*-}\ell^+\nu_\ell$ decays [4–10]. These analyses of the one-dimensional differential decay rate resulted in the measurement of only one of the form-factor parameters, and they relied on a measurement by the CLEO Collaboration [11] for the other two. The uncertainty in these two parameters introduces the largest systematic uncertainty in all previous measurements of $|V_{cb}|$ using this method.

Furthermore, for measurements of $|V_{ub}|$, based on both inclusive and exclusive $B \to X_u\ell\nu$ decays, improved knowledge of all form factors is important to correctly describe the dominant $B \to X_c\ell\nu$ background.

In this paper, we present a simultaneous measurement of $|V_{cb}|$, of the branching fraction for $B^0 \to D^{*-}\ell^+\nu_\ell$, and of the three form-factor parameters, based on measurements of three one-dimensional decay distributions. Thus we extend the earlier *BABAR* measurement [10] where $F(1)|V_{cb}|$ and one of the form-factor parameters are measured, fully accounting for correlations between these one-dimensional distributions.

We combine the results of this analysis with another *BABAR* measurement of the form factors [12], which employs a fit to the full four-dimensional decay distribution on a partial sample of the data.

The D^{*-} candidates are reconstructed from the $D^{*-} \to \bar{D}^0\pi^-$ decays, and the $\bar{D}^0$ mesons are reconstructed in three different decay modes, $K^+\pi^-$, $K^+\pi^-\pi^+\pi^-$, and $K^+\pi^-\pi^0$. Electrons or muons are paired with the D^{*-} to form signal candidates. The large data sample permits a precise determination of the background contributions, largely based on data, and thus results in smaller experimental uncertainties.

This leads to a further reduction of the form-factor errors.

II. FORMALISM

A. Kinematic variables

The lowest-order quark-level diagram for the decay $B^0 \to D^{*-}\ell^+\nu_\ell$ is shown in Fig. 1. This decay is completely characterized by four variables, namely, three angles and the Lorentz-invariant variable w, which is linearly related to q^2 and defined as

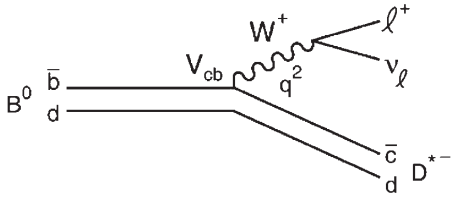

FIG. 1. Quark-level Feynman diagram for the decay $B^0 \to D^{*-}\ell^+\nu_\ell$.

$$w \equiv \frac{P_B \cdot P_{D^*}}{m_B m_{D^*}} = \frac{m_B^2 + m_{D^*}^2 - q^2}{2 m_B m_{D^*}}, \quad (1)$$

where m_B and m_{D^*} are the masses of the B and the D^* mesons (2.010 and 5.2794 GeV, respectively [13]), and P_B and P_{D^*} are their four-momenta. In the B rest frame the expression for w reduces to the Lorentz boost $\gamma_{D^*} = E_{D^*}/m_{D^*}$.

The ranges of w and q^2 are restricted by the kinematics of the decay, with $q^2 = 0$ corresponding to

$$w_{\max} = \frac{m_B^2 + m_{D^*}^2}{2 m_B m_{D^*}} = 1.504 \quad (2)$$

and $w_{\min} = 1$ corresponding to

$$q^2_{\max} = (m_B - m_{D^*})^2 = 10.69\ (\mathrm{GeV})^2. \quad (3)$$

The three angular variables, shown in Fig. 2, are as follows:

(i) θ_ℓ, the angle between the direction of the lepton in the virtual W rest frame and the direction of the W in the B rest frame;

(ii) θ_V, the angle between the direction of the D in the D^* rest frame and the direction of the D^* in the B rest frame;

(iii) χ, the angle between the plane formed by the D^* and the plane formed by the W decay.

B. Four-dimensional decay distribution

The Lorentz structure of the $B^0 \to D^{*-}\ell^+\nu_\ell$ decay amplitude can be expressed in terms of three helicity amplitudes (H_+, H_-, and H_0), which correspond to the three polarization states of the D^*, two transverse and one longitudinal. For low-mass leptons, these amplitudes are expressed in terms of the three functions $h_{A_1}(w)$, $R_1(w)$, and $R_2(w)$ [2,3]:

$$H_i(w) = m_B \frac{R^*(1-r^2)(w+1)}{2\sqrt{1-2wr+r^2}} h_{A_1}(w) \tilde{H}_i(w), \quad (4)$$

where

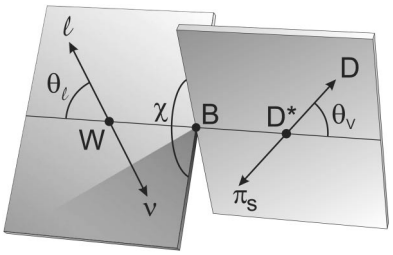

FIG. 2. Definition of the angles θ_ℓ, θ_V, and χ for the $B^0 \to D^{*-}\ell^+\nu_\ell$ decay, mediated by a vector boson W; π_s refers to the low-momentum pion from the decay $D^{*-} \to \bar{D}^0\pi_s^-$.

$$\tilde{H}_{\mp} = \frac{\sqrt{1-2wr+r^2}\left(1 \pm \sqrt{\frac{w-1}{w+1}} R_1(w)\right)}{1-r}, \quad (5)$$

$$\tilde{H}_0 = 1 + \frac{(w-1)(1-R_2(w))}{1-r}, \quad (6)$$

with $R^* = (2\sqrt{m_B m_{D^*}})/(m_B + m_{D^*})$ and $r = m_{D^*}/m_B$.

The functions $R_1(w)$ and $R_2(w)$ are defined in terms of the axial and vector form factors as

$$A_2(w) \equiv \frac{R_2(w)}{R^{*2}} \frac{2}{w+1} A_1(w), \quad (7)$$

$$V(w) \equiv \frac{R_1(w)}{R^{*2}} \frac{2}{w+1} A_1(w). \quad (8)$$

By convention, the function $h_{A_1}(w)$ is defined as

$$h_{A_1}(w) \equiv \frac{1}{R^*} \frac{2}{w+1} A_1(w). \quad (9)$$

For $w \to 1$, the axial form factor $A_1(w)$ dominates, and in the limit of infinite $b-$ and $c-$ quark masses, a single form factor describes the decay, the so-called Isgur-Wise function [14].

The fully differential decay rate in terms of the three helicity amplitudes is

$$\begin{aligned}\frac{d^4\Gamma(B^0 \to D^{*-}\ell^+\nu_\ell)}{dw\, d\cos\theta_\ell\, d\cos\theta_V\, d\chi} = {} & \frac{6 m_B m_{D^*}^2}{8(4\pi)^4}\sqrt{w^2-1}(1-2wr+r^2) G_F^2 |V_{cb}|^2 \{(1-\cos\theta_\ell)^2 \sin^2\theta_V H_+^2(w) \\ & + (1+\cos\theta_\ell)^2 \sin^2\theta_V H_-^2(w) + 4\sin^2\theta_\ell \cos^2\theta_V H_0^2(w) - 2\sin^2\theta_\ell \sin^2\theta_V \cos 2\chi H_+(w) H_-(w) \\ & - 4\sin\theta_\ell (1-\cos\theta_\ell)\sin\theta_V \cos\theta_V \cos\chi H_+(w) H_0(w) \\ & + 4\sin\theta_\ell (1+\cos\theta_\ell)\sin\theta_V \cos\theta_V \cos\chi H_-(w) H_0(w)\}. \end{aligned} \quad (10)$$

By integrating this decay rate over all but one of the four variables, w, $\cos\theta_\ell$, $\cos\theta_V$, or χ, we obtain the four one-dimensional decay distributions from which we extract the form factors. The differential decay rate as a function of w is

$$\frac{d\Gamma}{dw} = \frac{G_F^2}{48\pi^3} m_{D^{*+}}^3 [m_{\bar{B}^0} - m_{D^{*+}}]^2 \mathcal{G}(w) \mathcal{F}^2(w) |V_{cb}|^2, \quad (11)$$

where

$$\mathcal{F}^2(w)\mathcal{G}(w) = h_{A_1}^2(w)\sqrt{w-1}(w+1)^2 \times \left\{2\left[\frac{1-2wr+r^2}{(1-r)^2}\right]\left[1+R_1(w)^2\frac{w-1}{w+1}\right] + \left[1+(1-R_2(w))\frac{w-1}{1-r}\right]^2\right\},$$

and $\mathcal{G}(w)$ is a known phase space factor,

$$\mathcal{G}(w) = \sqrt{w^2-1}(w+1)^2\left[1+4\frac{w}{w+1}\frac{1-2wr+r^2}{(1-r)^2}\right].$$

It is important to note that $h_{A_1}(1) \equiv \mathcal{F}(1)$ corresponds to the Isgur-Wise function [14] at $w = 1$. In the infinite quark-mass limit, the HQS normalization gives $\mathcal{F}(1) = 1$. Corrections to this HQS prediction have been calculated in the framework of lattice QCD. A recent calculation, performed in a quenched approximation, predicts (including a QED correction of 0.7%) $\mathcal{F}(1) = 0.919^{+0.030}_{-0.035}$ [15]. This value is compatible with estimates based on nonlattice methods [16,17].

C. Form-factor parametrization

Since HQET does not predict the functional form of the form factors, a parametrization is needed for their extraction from the data. Perfect heavy-quark symmetry implies that $R_1(w) = R_2(w) = 1$, i.e., the form factors A_2 and V are identical for all values of w and differ from A_1 only by a simple kinematic factor. Corrections to this approximation have been calculated in powers of $(\Lambda_{\rm QCD}/m_b)$ and the strong coupling constant α_s. Various parametrizations in powers of $(w-1)$ have been proposed. Among the different predictions relating the coefficients of the higher order terms to the linear term, we adopt the following expressions derived by Caprini, Lellouch, and Neubert [18],

$$h_{A_1}(w) = h_{A_1}(1)[1 - 8\rho^2 z + (53\rho^2 - 15)z^2 - (231\rho^2 - 91)z^3], \quad (12)$$

$$R_1(w) = R_1(1) - 0.12(w-1) + 0.05(w-1)^2, \quad (13)$$

$$R_2(w) = R_2(1) + 0.11(w-1) - 0.06(w-1)^2, \quad (14)$$

where $z = [\sqrt{w+1} - \sqrt{2}]/[\sqrt{w+1} + \sqrt{2}]$.

The three parameters, ρ^2, $R_1(1)$, and $R_2(1)$, cannot be calculated; they must be extracted from data.

III. DATA SAMPLE, RECONSTRUCTION, AND SIMULATION

The data used in this analysis were recorded by the *BABAR* detector, operating at the PEP-II asymmetric-energy e^+e^- collider. The data sample corresponds to a luminosity of 79 fb^{-1} recorded on the $\Upsilon(4S)$ resonance (on-resonance sample), and 9.6 fb^{-1} recorded at a center-of-mass energy 40 MeV lower (off-resonance sample).

The *BABAR* detector and event reconstruction have been described in detail elsewhere [19,20]. The momenta of charged particles are measured by a tracking system consisting of a five-layer silicon vertex tracker (SVT) and a 40-layer drift chamber (DCH). Charged particles of different masses are distinguished by their energy loss in the tracking devices and by a ring-imaging Cerenkov detector (DIRC). Electromagnetic showers from electrons and photons are measured in a CsI(Tl) calorimeter (EMC). These detector components are embedded in a 1.5-T magnetic field of the solenoid. Electron candidates are selected on the basis of the ratio of the energy detected in the calorimeter to the track momentum, the calorimeter shower shape, the energy loss in the drift chamber, and the angle of the photons reconstructed in the DIRC. Muons are identified in a set of resistive plate chambers inserted in the steel flux-return of the magnet (IFR). Information from the IFR is combined with the track momentum measurement and energy deposition in the EMC to improve the separation of muons from charged hadrons.

The electron and muon identification efficiencies and the probabilities to misidentify a pion, kaon, or proton as an electron or muon have been measured as a function of the laboratory momentum and the angles with clean samples of tracks selected from data [21]. Within the acceptance of the calorimeter, defined by the polar angle in the laboratory frame, $-0.72 < \cos\theta_{\rm lab} < 0.92$, and above 1.0 GeV, the average electron efficiency is 91%, largely independent of the electron momentum. The average hadron misidentification rate is less than 0.2%. The muon detection extends to polar angles of $-0.91 < \cos\theta_{\rm lab} < 0.95$. For a hadron misidentification rate of typically 2.0%, the average efficiency is close to 65%.

The criteria for distinguishing charged kaons from charged pions are chosen to maximize the efficiency while controlling the background, and thus differ for the decay modes under study. Consequently, the efficiency varies from 87% to 97%. The uncertainties are typically 1%.

We determine the tracking efficiency for high-momentum tracks by comparing the independent information from SVT and DCH. We compute the efficiency for low-momentum tracks reconstructed in the SVT alone from the angular distribution of the ''slow'' pion, π_s^-, in the D^{*-} rest frame. We use a large sample of $D^{*-} \to \bar{D}^0\pi_s^-$, $\bar{D}^0 \to K^+\pi^-$ decays selected from hadronic B decays. For fixed values of the D^{*-} momentum, we compare the observed angular distribution to the one expected for the decay of a vector meson to two pseudoscalar mesons. This study is performed in several bins of the polar angle. We define the relative efficiency as the ratio of the observed to the expected distribution and parametrize its dependence on the laboratory momentum of the π_s^-. Below 100 MeV, this efficiency drops very steeply, and reaches zero at about 60 MeV.

Neutral pions are reconstructed from pairs of photon candidates of more than 30 MeV detected in the EMC

and assumed to originate from the interaction point. For photon pairs with an invariant mass within 15.75 MeV of the nominal π^0 mass, we perform a kinematic fit, constraining the mass. We require that the probability of the fit exceeds 1%. The efficiencies, including the EMC acceptance, vary between 55% and 65% for π^0 energies ranging from 0.3 to 2.5 GeV, for a mass resolution between 5.5 and 7.5 MeV.

We use Monte Carlo (MC) simulation of the production and decay of B mesons at the $\Upsilon(4S)$ resonance and of the detector response [22] to estimate signal and background efficiencies, and to extract the observed signal and background distributions to fit the data. We assume that the $\Upsilon(4S)$ decays exclusively to $B\bar{B}$ pairs. The simulated sample of generic $B\bar{B}$ events corresponds to roughly 3 times the $B\bar{B}$ data sample.

Information from studies of selected control data samples on efficiencies and resolutions is used to improve the accuracy of the simulation. Comparisons of data with the MC simulations have revealed small differences in the tracking and particle detection efficiencies, which have been corrected for. The MC simulations include radiative effects such as bremsstrahlung in the detector material. QED final state radiation is modeled by PHOTOS [23], and decays with radiative photons are included in the signal sample.

In the MC simulations the branching fractions for hadronic B and D decays are based on average values reported in the Review of Particle Physics [13]. $B^0 \to D^{*-}\ell^+\nu_\ell$ signal events are generated with the HQET-based form factors, using the specific parametrization by Caprini, Lellouch, and Neubert [18]. Values of the form-factor parameters are taken from measurements by the CLEO Collaboration [11]. $B \to D^{**}\ell\nu$ decays, involving orbitally excited charm mesons, are generated according to the ISGW2 model [24], and decays to nonresonant charm states are generated following the prescription of Goity and Roberts [25].

IV. EVENT SELECTION AND BACKGROUND SUBTRACTION

A. Event selection

The reconstruction of the events and the selection of candidate $B^0 \to D^{*-}\ell^+\nu_\ell$ decays are largely common to the earlier *BABAR* analysis [10].

We select events that contain a D^{*-} candidate and an oppositely charged electron or muon with momentum in the range $1.2 < p_\ell < 2.4$ GeV. Unless explicitly stated otherwise, momenta are measured in the $\Upsilon(4S)$ rest frame, which is boosted relative to the laboratory frame, $\beta\gamma = 0.56$. We reconstruct D^{*-} in the decay channel $D^{*-} \to \bar{D}^0\pi_s^-$, with the $\bar{D}^0$ decaying to $K^+\pi^-$, $K^+\pi^-\pi^+\pi^-$, or $K^+\pi^-\pi^0$. The tracks of the charged hadrons from the $\bar{D}^0$ candidate are fitted to a common vertex, and the candidate is rejected if the fit probability is less than 0.1%. We require the invariant mass of the hadrons to be compatible with the $\bar{D}^0$ mass within ± 2.5 times the experimental resolution, corresponding to ± 34 MeV for $\bar{D}^0 \to K^+\pi^-\pi^0$ decays and ± 17 MeV for the other decays. For the decay $\bar{D}^0 \to K^+\pi^-\pi^0$, we accept only candidates from portions of the Dalitz plot where the square of the decay amplitude [26] exceeds 10% of the maximum. We select D^{*-} candidates with a momentum in the range $0.5 < p_{D^*} < 2.5$ GeV. For the π_s^- from the D^{*-} decay, the momentum in the laboratory frame must be less than 450 MeV, and the momentum transverse to the beam must be greater than 50 MeV. Finally, the lepton, the π_s^-, and the $\bar{D}^0$ are fitted to a common vertex using a constraint from the beam-beam interaction point. The probability for this fit is required to exceed 1%.

In semileptonic decays, the presence of an undetected neutrino complicates the separation of the signal from background. For a signal B^0 decay, the D^{*-} and the charged lepton originate from the B^0 and the only missing particle is a massless neutrino. The absolute value of the B momentum, p_B, is known from the total energy in the event, and its direction is constrained to lie on a cone centered on the $D^{*-}\ell^+$ momentum vector. The opening angle of this cone, $\theta_{B,D^*\ell}$, is computed for each event,

$$\cos\theta_{B,D^*\ell} = \frac{2E_B E_{D^*\ell} - m_B^2 - m_{D^*\ell}^2}{2p_B p_{D^*\ell}}. \qquad (15)$$

Here m, E, and p refer to the mass, the energy, and the absolute value of the momentum. The condition $|\cos\theta_{B,D^*\ell}| \leq 1.0$ should be fulfilled in a perfectly reconstructed decay. The value of w depends on the azimuthal angle of the B^0 direction, which cannot be determined. We therefore approximate w by the average of the four values of w corresponding to the azimuthal angles 0, $\pi/2$, π, and $3\pi/2$, as was done in [12]. This approximation results in an average resolution for w of 0.04.

B. Background subtraction

The background subtraction is performed separately for each of the four kinematic variables (w, $\cos\theta_\ell$, $\cos\theta_V$, and χ), to be used for the extraction of the form-factor parameters and $|V_{cb}|$. For each variable, we divide the events into ten subsets, each corresponding to one of ten bins of the distribution, and the fits are performed separately for the ten subsets.

The selected events are divided into six signal samples by separating decays into electrons and muons and the three $\bar{D}^0$ decay modes. In addition to signal events, each subsample contains background events from six different sources:

(i) *combinatorial background* (events from $B\bar{B}$ and continuum $q\bar{q}$ production in which at least one of the hadrons assigned to the D^{*-} does not originate from the D^{*-} decay);

(ii) *continuum background* ($D^{*-}\ell^+$ combinations from $e^+e^- \to c\bar{c}$);
(iii) *fake-lepton background* (a true D^{*-} combined with a hadron misidentified as a lepton);
(iv) *uncorrelated background* (ℓ^+ and D^{*-} originating from the decay of two different B mesons);
(v) *B background involving higher-mass charm states*, either $B^+ \to D^* X \ell^+ \nu_\ell$ decays (via $B^+ \to \bar{D}^{**0}\ell^+\nu_\ell$ or nonresonant $B^+ \to D^{*-}\pi^+\ell^+\nu_\ell$ charm states), or $B^0 \to D^{*-} X \ell^+ \nu_\ell$ decays (via $B^0 \to D^{**-}\ell^+\nu_\ell$ or nonresonant $B^0 \to D^{*-}\pi^0\ell^+\nu_\ell$ charm states);
(vi) *correlated background events* due to the processes $B^0 \to D^{*-}\tau^+\nu_\tau$ with $\tau^+ \to \ell^+ X$, and $B^0 \to D^{*-} X_c$ with $X_c \to \ell^+ Y$.

Except for the combinatorial background, all background sources contain a true $D^{*-} \to \bar{D}^0\pi_s^-$ decay and thus are expected to exhibit a peak in the $\Delta m = m_{D^{*-}} - m_{\bar{D}^0}$ distribution, where $m_{D^{*-}}$ and $m_{\bar{D}^0}$ are the reconstructed masses of the D^{*-} and $\bar{D}^0$ candidates. We determine the background distributions from data, except for the correlated background, which amounts to less than 1.8% of the total sample of selected candidates.

We determine the signal and background composition in two steps. First, we estimate the combinatorial, the continuum, and the fake-lepton background from fits to the Δm distributions (Fig. 3). Second, we fix the background levels for these three sources and determine the uncorrelated background and the $B \to D^* X \ell \nu_\ell$ background from fits to the $\cos\theta_{B,D^*\ell}$ distributions (Fig. 4). The shape and normalization of the small correlated background is fixed to the MC predictions and based on measured branching fractions [13].

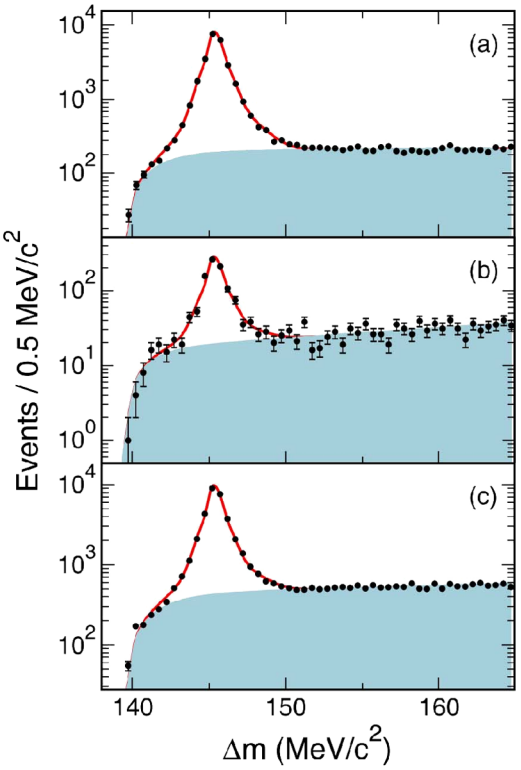

FIG. 3 (color online). Δm distributions for the decays $D^{*-} \to \bar{D}^0\pi_s^-$ with $\bar{D}^0 \to K^+\pi^-$ for events in which the π_s^- track is reconstructed in the SVT only, (a) for on-resonance, (b) for off-resonance data in which an electron or muon was identified, and (c) for on-resonance data in which no charged lepton was found in the event. The data (points with statistical errors), integrated over the full w range, are compared to the result of the simultaneous fit (solid line) to all three distributions. The shaded area shows the fitted combinatorial background; the remainder (white area) represents the sum of the signal and peaking backgrounds.

1. Fits to Δm distributions

To estimate the shape and normalization of the combinatorial, the continuum, and fake-lepton backgrounds from the measured Δm distributions, we use, in addition to the on-resonance data, off-resonance data, as well as a set of on-resonance events in which no lepton is identified and a charged hadron is selected to take its place. We refer to this data sample as the fake-lepton sample. For each of these data sets, we perform an unbinned maximum-likelihood fit to the Δm distributions. The data are fitted to a sum of a peak, due to correctly reconstructed $D^{*-} \to \bar{D}^0\pi_s^-$ decays, and a combinatorial background.

The peak is described as a sum of three Gaussian resolution functions with three mean values, three different widths, and two parameters that specify the contributions of continuum and fake-lepton backgrounds relative to the total number of events above the combinatorial background. The combinatorial background is described, as in [10], by an empirical function,

$$F_{\mathrm{comb}}(\Delta m) = \frac{1}{N}\left[1 - e^{-[(\Delta m - \Delta m_0)/c_1]}\right]\left(\frac{\Delta m}{\Delta m_0}\right)^{c_2}, \quad (16)$$

where N is the normalization, Δm_0 refers to the kinematic threshold equal to the pion mass, and c_1 and c_2 are free parameters.

Since the Δm resolutions and background yields depend on the $\bar{D}^0$ decay mode, and on whether the low-momentum pion track is reconstructed in the SVT alone or in both SVT and DCH, the parameters describing the peak contributions are determined separately for the three subsamples corresponding to the $\bar{D}^0$ decay modes, each divided into two classes of events, depending on the detection of the slow pion.

The off-resonance distributions are scaled to the on-resonance luminosity, and the simulated lepton signal and fake-lepton samples are adjusted to reproduce the detection efficiencies and misidentification probabilities determined from independently selected data control samples. For the on- and off-resonance data and for the fake-lepton sample, the parameters describing the shape and normalization of the combinatorial background differ, and they are therefore determined separately, while the

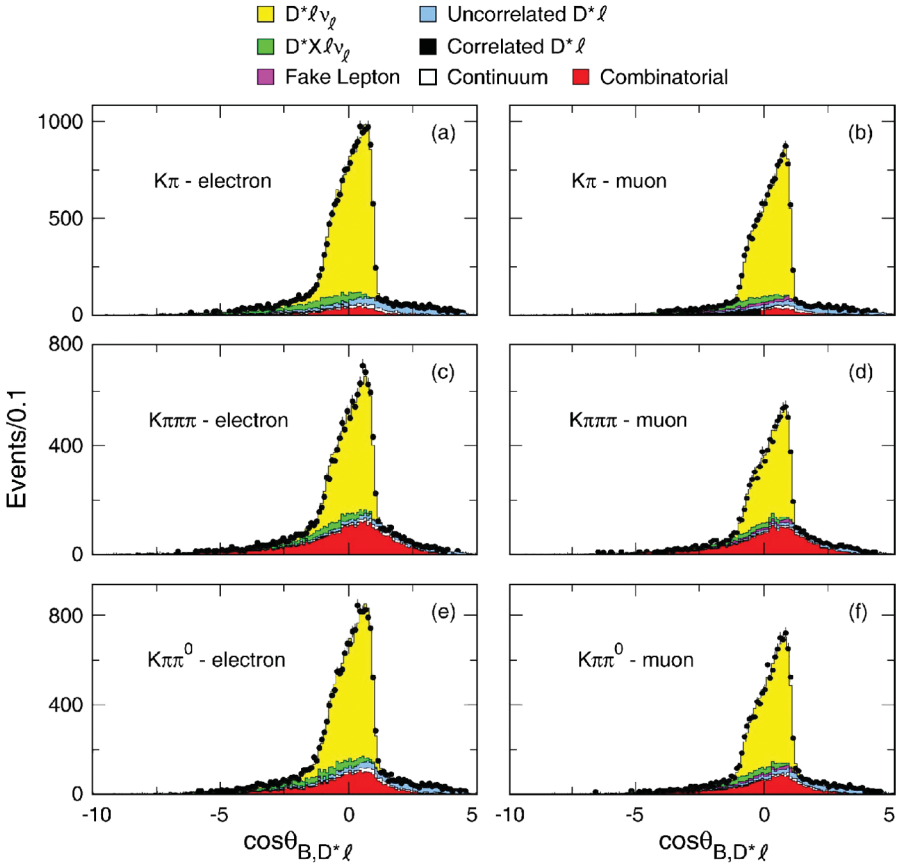

FIG. 4 (color). The $\cos\theta_{B,D^*\ell}$ distributions (points with statistical errors) for selected events in the six subsamples (integrated over the full range in w): (a,b) $D \to K\pi$, (c,d) $D \to K\pi\pi\pi$, and (e,f) $D \to K\pi\pi^0$, compared to the result of the fits to signal and background contributions.

mean and the widths of the Gaussian functions are common.

The fits extend in Δm from 138 to 165 MeV. Given the very large number of parameters and the many data subsamples and various subsets, the fits to the Δm distributions are performed in several steps. Initially, the parameters describing the combinatorial background contributions are fixed to values determined from binned χ^2 fits to simulated distributions. With these starting values for the combinatorial background shapes, an unbinned maximum-likelihood fit is performed to all subsets of the data, both on- and off-resonance, to determine the eight peak-shape variables and three additional relative peak yields for each data subset. To improve the agreement with the data, the parameters describing the combinatorial background distributions are then refitted, together with the three peak yield parameters, with the remaining parameters describing the components of the peaking signal and background fixed to the results of the previous fit.

As an illustration for these background fits, Fig. 3 shows the Δm distributions for the decays $D^{*-} \to \bar{D}^0 \pi_s^-$ with $\bar{D}^0 \to K^+ \pi^-$ for events in which the π_s^- track is reconstructed in the SVT only. The data are compared to the results of the combined fit to three distributions, for selected samples of on-resonance data, off-resonance data, and on-resonance data without an identified lepton.

The fitted fractions of combinatorial, fake-lepton, and continuum background events are determined for the peak regions in Δm, which are defined as 144 to 147 MeV for events with the slow charged pion detected in the SVT and DCH, and 143 to 148 MeV for decays with the π_s^- detected in the SVT alone.

2. *Fits to* $\cos\theta_{B,D^*\ell}$ *distributions*

In a second step, a binned χ^2 fit is performed to the $\cos\theta_{B,D^*\ell}$ distributions in the range $-10 < \cos\theta_{B,D^*\ell} < 5$, to determine the signal contribution and the normalization of the uncorrelated and $B \to D^* X \ell \nu_\ell$ background events. Neglecting resolution and radiative effects, signal events meet the constraint $|\cos\theta_{B,D^*\ell}| \leq 1$, while the distribution of $B \to D^* X \ell \nu_\ell$ events extends below -1, and the uncorrelated background events are spread over the entire range considered. Because of final state radiation, the events in the electron samples also contribute to lower values of $\cos\theta_{B,D^*\ell}$.

This fit is performed separately for the six signal samples, corresponding to the $\bar{D}^0$ mesons reconstructed

TABLE I. Number of selected candidates and background fractions, separately for the subsamples identified by the $\bar{D}^0$ decay mode and the charged lepton.

Subsamples	$K\pi e$	$K\pi\mu$	$K\pi\pi\pi e$	$K\pi\pi\pi\mu$	$K\pi\pi^0 e$	$K\pi\pi^0\mu$
Number of selected candidates	15 144	12 083	10 259	7831	13 224	10 299
Signal fraction (%)	85.27 ± 0.31	83.27 ± 0.37	69.25 ± 0.54	66.30 ± 0.66	75.72 ± 0.43	74.05 ± 0.50
Background source	Background fractions (%)					
$B \to D^* X \ell \nu_\ell$	3.89 ± 0.16	3.93 ± 0.18	3.76 ± 0.19	3.74 ± 0.22	4.05 ± 0.17	4.08 ± 0.20
Fake leptons	0.23 ± 0.04	2.45 ± 0.14	0.12 ± 0.03	2.29 ± 0.17	0.22 ± 0.04	2.41 ± 0.15
Uncorrelated	3.59 ± 0.15	3.11 ± 0.16	2.71 ± 0.16	2.27 ± 0.17	3.38 ± 0.16	3.29 ± 0.18
Correlated	0.37 ± 0.05	0.56 ± 0.07	0.36 ± 0.06	0.48 ± 0.08	0.35 ± 0.05	0.47 ± 0.07
Continuum	1.80 ± 0.11	2.08 ± 0.13	1.82 ± 0.13	1.43 ± 0.14	1.83 ± 0.12	1.60 ± 0.12
Combinatorial	4.85 ± 0.18	4.60 ± 0.20	21.98 ± 0.46	23.49 ± 0.55	14.45 ± 0.33	14.10 ± 0.37

in three different decay modes, divided into events with electrons or muons. Each signal sample is further divided into ten subsets corresponding to ten bins in one of the four kinematic variables. We perform the fits separately for each bin, with the individual shapes for the signal and for each of the six background sources taken from MC simulation. The fraction of the combinatorial, fake-lepton, and continuum events are taken from the Δm fits and fixed.

To reduce the sensitivity to statistical fluctuations, we require that the ratio of $B \to D^* X \ell \nu_\ell$ background and of uncorrelated background to the signal be the same for all three $\bar{D}^0$ decay modes, with either electrons or muons. The $\cos\theta_{B,D^*\ell}$ distributions for the six signal samples and the results of the fits are shown in Fig. 4. In total, there are 68 840 decay candidates in the range $|\cos\theta_{B,D^*\ell}| < 1.2$. The number of selected events and the fractions of background events are given in Table I. As expected, the fake rate is about a factor 10 higher for decays to muons than to electrons. Except for the combinatorial backgrounds, which vary significantly for the three $\bar{D}^0$ decays modes, most of the other background fractions are similar for the six data samples.

V. EXTRACTION OF $|V_{cb}|$ AND FORM-FACTOR PARAMETERS

We determine $\mathcal{F}(1)|V_{cb}|$ and the three form-factor parameters by extending the one-dimensional least-squares fit to the w distribution used previously [10] to a combined fit of three one-dimensional binned distributions, with bin-by-bin background subtraction. We have chosen this approach to avoid the statistical limitations of a fit to a binned four-dimensional decay distribution.

In principle, any kinematic observable that is sensitive to the form-factor parameters can be used. We have examined the sensitivity of the four kinematic variables, w, $\cos\theta_\ell$, $\cos\theta_V$, and χ (see Sec. II), to the form-factor parameters and found that the χ distribution is practically insensitive, and thus we select the remaining three variables. As done for the background estimate, we again divide the distributions into ten bins with equal bin size for w and $\cos\theta_V$, and varying bin size for $\cos\theta_\ell$ in order to have a more similar population in all the bins for this variable.

We perform a least-squares fit to these three projected one-dimensional distributions to extract the form factors and $\mathcal{F}(1)|V_{cb}|$, using the independently determined background estimates. We account for the correlations by noting that the statistical covariance between the content of two bins in two different one-dimensional distributions is determined by the common number of events in these bins, while it is zero for bins in the same distribution. Since each of the three distributions that are included in the fit contain the same events and thus have the same normalization, we reduce the total number of bins used in the fit by 2, from 30 to 28. The choice of the bins that are left out is arbitrary, and it has been verified that the fit result does not depend on this choice.

A. The least-squares fit

The concept for this fit is an extension of the one introduced in the previous *BABAR* analysis [10]. For a given bin with index i, $N_i^{\rm data}$ is the total number of observed events, $N_i^{\rm bkg}$ is the estimated number of background events, and $N_i^{\rm MC}$ refers to the number of MC-simulated signal events. The fit function can be written as

$$X^2 = \sum_{i=1}^{n_{\rm bin}=28} \sum_{j=1}^{n_{\rm bin}=28} \left(N_i^{\rm data} - N_i^{\rm bkg} - \sum_{k=1}^{N_i^{\rm MC}} \mathrm{W}_i^k \right) \times C_{ij}^{-1} \left(N_j^{\rm data} - N_j^{\rm bkg} - \sum_{k=1}^{N_j^{\rm MC}} \mathrm{W}_j^k \right), \quad (17)$$

where the indices i and j run over the 28 bins, and the index k runs over all MC-simulated events, $N_i^{\rm MC}$, in bin i. W_i^k is a weight assigned to the kth simulated signal event in bin i to evaluate the expected signal yield as a function of the free parameters of the fit, and C_{ij} is the covariance matrix element for a pair of bins i and j.

Each weight W_i^k is the product of four weights, $\mathrm{W}_i^k = \mathrm{W}_i^{ff,k} \mathrm{W}^{\mathcal{L}} \mathrm{W}_i^{\epsilon,k} \mathrm{W}_i^{S,k}$.

(1) The factor $W_i^{ff,k}$ accounts for the dependence of the signal yield on the parameters to be fitted. The $|V_{cb}|$ dependence is trivially given by the ratio $|V_{cb}|^2/|V_{cb}^{MC}|^2$, where the denominator is the actual value used in the simulation, derived from the branching fraction assumed for the decay $B^0 \to D^{*-}\ell^+\nu_\ell$. Similarly, the dependence on the form-factor parameters, ρ^2, $R_1(1)$, and $R_2(1)$, is given by the ratio of the differential decay rate [Eq. (10)], evaluated for the values assigned during the fit and for the values adopted in the simulation.

(2) The factor $W^{\mathcal{L}}$ accounts for the relative normalization of data and simulated samples. It is the product of the following terms:
   (i) the ratio of the total number of $B\bar{B}$ events, $N_{B\bar{B}} = (85.9 \pm 0.9) \times 10^6$, and the number of Monte Carlo events for the final states $B^0\bar{B}^0$ and B^+B^-;
   (ii) the ratios $1/[1 + f_{+-}/f_{00}]$ for B^0, $[f_{+-}/f_{00}]/[1 + f_{+-}/f_{00}]$ for B^+, where $f_{+-}/f_{00} = \mathcal{B}(\Upsilon(4S) \to B^+B^-)/\mathcal{B}(\Upsilon(4S) \to B^0\bar{B}^0) = 1.037 \pm 0.029$ [13] is the ratio of the number of charged to neutral B mesons produced;
   (iii) the ratio of the $c\bar{c}$ to $b\bar{b}$ pair-production cross section;
   (iv) the ratio of the branching fraction $\mathcal{B}(D^{*-} \to \bar{D}^0\pi^-) = 0.677 \pm 0.005$ [13] and of the B^0 lifetime $\tau_{B^0} = 1.530 \pm 0.009$ ps [13] to the values used in the Monte Carlo simulation.

The uncertainties on the measured quantities used in this weight function are not accounted for in the fit; their impact is studied by repeating the fit with their values changed by 1 standard deviation.

(3) The factor $W_i^{\epsilon,k}$ is the product of the correction factors for efficiencies, applied on a particle-by-particle basis, which accounts for the residual differences in reconstruction and particle-identification efficiencies between the data and the Monte Carlo simulation, as a function of particle momentum and polar angle.

(4) The factor $W_i^{S,k}$ accounts for potential small differences in efficiencies among the six data subsamples and allows the adjustment of the $\bar{D}^0$ branching fractions, properly accounting for their correlated systematic uncertainties. $W_i^{S,k}$ is the product of several scale factors that are free parameters in the fit, each constrained to its expected value within the estimated experimental uncertainty. Specifically, to account for the uncertainty in the multiplicity-dependent tracking efficiency, we introduce a factor $W_{trk}^S = 1 + N_{trk}(1 - \delta_{trk})$, where N_{trk} is the number of charged tracks of the $D^*\ell$ candidates and δ_{trk} is constrained to 1.0 within the estimated uncertainty of $\sigma_{trk} = 0.8\%$ in the single-track efficiency. Similarly, multiplicative correction factors δ_ℓ, δ_K, and δ_{π^0} are introduced to adjust the efficiencies for leptons (δ_e for $e^\pm$ or δ_μ for $\mu^\pm$), kaons, and π^0 mesons, each within their estimated uncertainties, σ_ℓ (σ_e for $e^\pm$ or σ_μ for $\mu^\pm$), σ_K, and σ_π. Likewise, $\delta_{\mathcal{B}(K\pi)}$, $\delta_{\mathcal{B}(K\pi\pi\pi)}$, $\delta_{\mathcal{B}(K\pi\pi^0)}$ are introduced to adjust the individual $\bar{D}^0$ branching fractions within their current measurement uncertainties [13]. Correlations between the branching fraction measurements are taken into account by the covariance matrix $C_{\mathcal{B}}$.

As a result, $W_i^{S,k}$ can be expressed as

$$W_i^{S,k} = \delta_\ell^{i,k}\delta_K^{i,k}(1 + N_{trk}^{i,k}(1 - \delta_{trk}))\delta_{\pi^0}^{i,k}\delta_{\mathcal{B}}^{i,k}.$$

The corrections to the kaon and π^0 efficiency, the decay multiplicity, N_{trk}, and the $\bar{D}^0$ branching fraction depend on the particular event k in bin i.

The complete ansatz for the X^2 function used in the fit is

$$\begin{aligned} X^2 = & \sum_{i=1}^{n_{bin}=28}\sum_{j=1}^{n_{bin}=28}\left[\left(N_i^{data} - N_i^{bkg} - \sum_{k=1}^{N_i^{MC}} W_i^k\right)\right. \\ & \left.\times C_{ij}^{-1}\left(N_j^{data} - N_j^{bkg} - \sum_{k=1}^{N_j^{MC}} W_j^k\right)\right] \\ & + \frac{(1-\delta_\ell)^2}{\sigma_\ell^2} + \frac{(1-\delta_K)^2}{\sigma_K^2} + \frac{(1-\delta_{trk})^2}{\sigma_{trk}^2} \\ & + \frac{(1-\delta_{\pi^0})^2}{\sigma_{\pi^0}^2} + \sum_{m=1}^{3}\sum_{n=1}^{3}\delta_{\mathcal{B}(m)} \times C_{\mathcal{B}(mn)}^{-1}\delta_{\mathcal{B}(n)}. \end{aligned} \quad (18)$$

The indices n, m refer to the three $\bar{D}^0$ decay modes. The addition of these extra terms allows us to fit all subsamples simultaneously, while taking into account the correlated systematic uncertainties and effectively propagating these uncertainties, via the weights, to the uncertainties on the free parameters of the fit.

The fit procedure has been tested on a large variety of Monte Carlo generated signal samples. The fits are performed for multiple samples, comparable in size to the data. The resulting pulls are consistent with a Gaussian distribution, with no evidence for systematic biases. The width of the pull distribution has been found to be consistent with 1, giving confidence in the uncertainty extracted from the fit.

B. The covariance matrix

A direct consequence of this method is that the covariance matrix for the measurements is not diagonal, since the events in different bins are not all statistically independent. The total covariance matrix is the sum of three separate matrices: one for the measured data yields, and one each for the estimated signal and background yields. The diagonal elements of the matrices are the uncertainties of the bin

contents. The covariance of bins belonging to the same distribution is zero, and the covariance of bins from different distributions is the variance of the number of events that is common for the two bins.

For the data, the covariance matrix is determined under the assumption that the data obey Poisson statistics, and therefore the variance of the bin or of the intersection of two bins is simply the number of events. The estimated signal matrix is built in an analogous way, where the variance of a number of weighted events n is approximated by the sum of the squares of the weights, $\sum_{i=1,n} w_i^2$.

The calculation of the background covariance matrix is less straightforward. The diagonal elements are simply the estimated variances of the measured background, according to the procedure described in Sec. IV. However, the background extraction procedure does not directly determine the number of common events in two bins, because this procedure is based on a rather complex sequence of fits to shapes and event yields. The solution adopted here is to use the number of common background events in two bins as predicted by the simulation, corrected for tracking and particle-identification (PID) efficiencies and adjustments to account for the background estimates. This is done in such a way that for each bin of one of the kinematic observables the background is equal to the data-based background estimate. The choice of the observable (w, $\cos\theta_\ell$, $\cos\theta_V$, or χ) is arbitrary, and the variation of the results with this choice is used to evaluate the systematic uncertainty introduced by this procedure.

Since the total number of background events estimated for the four different distributions is not exactly the same, we average the results obtained for the four distributions. The spread of the background normalization values is found to be almost twice as large as the estimated uncertainty from the error propagation. This can be explained by the fact that the uncertainties of the assumed signal and background shapes in the Δm fits are not accounted for in this propagation. We derive an estimate of this additional uncertainty using the number of background events determined from the fits to the background distributions. They are very similar for w and $\cos\theta_\ell$, and for $\cos\theta_V$ and χ. The estimate is given by the average of the minimum and maximum difference between these two groups.

VI. THE FIT RESULTS AND SYSTEMATIC UNCERTAINTIES

A. Results of the fit

The results of the simultaneous fit to the three one-dimensional distributions are presented in Table II. The stated uncertainties on ρ^2, $R_1(1)$, $R_2(1)$, and $\mathcal{F}(1)|V_{cb}|$ are taken from the MINUIT minimization program [27]. Among the form-factor parameters, the correlations are quite large, but their correlation with $\mathcal{F}(1)|V_{cb}|$ is less than 0.23. All the δ parameters are found to be consistent with their nominal value of 1 within their uncertainties.

TABLE II. The results of the fit: The parameters, their uncertainties, and the off-diagonal elements of the correlation matrix. The stated uncertainties include systematic ones that are not common to all events and are therefore included in the fit (see Sec. VI B 1).

Parameters	Fitted values	Correlations ρ^2	$R_1(1)$	$R_2(1)$
$\mathcal{F}(1)\|V_{cb}\|$	$(34.67 \pm 0.86) \times 10^{-3}$	-0.001	-0.196	$+0.141$
ρ^2	1.157 ± 0.095		$+0.867$	-0.924
$R_1(1)$	1.327 ± 0.131			-0.928
$R_2(1)$	0.859 ± 0.077			

Figure 5 compares the one-dimensional projections for the kinematic observables with the results of the fit, detailing the signal and background contributions. To provide an additional check on the background estimation, we also show the χ projection. The goodness of the fit, ignoring that the measurements used are not all independent, can be stated as $\chi^2/\text{d.o.f} = 23.8/24$, corresponding to a probability of 47.3%.

The $B^0 \to D^{*-}\ell^+\nu_\ell$ branching fraction, obtained by integrating the data over the full phase space, is found to be $\mathcal{B}(B^0 \to D^{*-}\ell^+\nu_\ell) = (4.72 \pm 0.05)\%$.

As a cross check, we perform the fit separately for the six subsamples. The quality of the fits is generally good, and the results, shown in Table III, agree within the uncertainties obtained, with the possible exception of the $K\pi\pi\pi e$ sample. Detailed investigations of the background estimates and fits for this sample did not reveal any anomalies.

B. Systematic uncertainties

A summary of statistical and systematic uncertainties on the measured parameters is presented in Table IV, including the breakdown of those for the measurement of the $B^0 \to D^{*-}\ell^+\nu_\ell$ branching fraction.

1. Uncertainties included in the fit

The uncertainty of the parameters resulting from the fit is not purely statistical, since the systematic uncertainty sources that are not common to all events are accounted for in the fit through the δ parameters in the weights $W_i^{S,k}$. As described above, these weights account for residual uncertainties in the lepton and hadron identification, the charged particle tracking and π^0 efficiencies, and the individual $\bar{D}^0$ branching fractions. We can determine the statistical uncertainties of the fit by repeating the fit with all δ parameters fixed at their fitted value. The systematic uncertainties are then obtained by subtracting the statistical covariance matrix from the total covariance matrix. While the uncertainties related to the detector performance are relatively

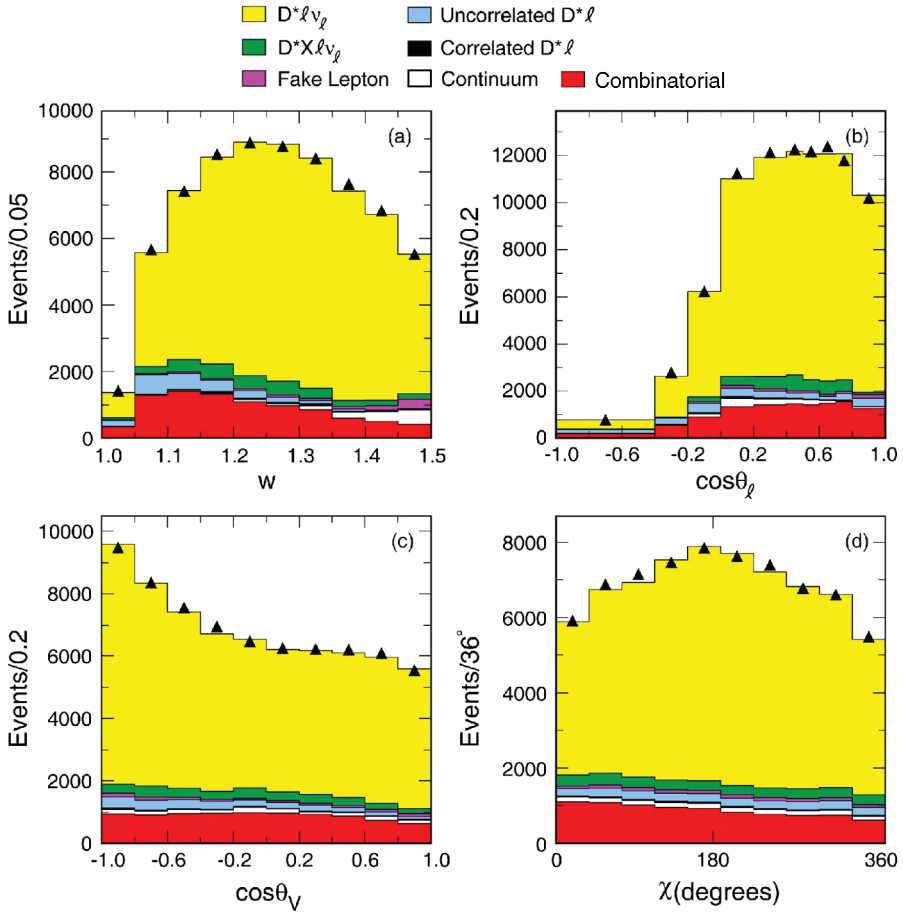

FIG. 5 (color). Comparison of the measured distributions (data points), (a) w, (b) $\cos\theta_\ell$, (c) $\cos\theta_V$, and (d) χ, with the result of the fit, shown as the sum of the fitted signal yield and the estimated background distributions. The statistical uncertainties of the data are too small to be visible.

small for the form-factor parameters, they are dominant for $\mathcal{F}(1)|V_{cb}|$ (2.5%) and the branching fraction (5.2%).

2. Soft pion efficiency

A major source of uncertainty on $\mathcal{F}(1)|V_{cb}|$ is the reconstruction efficiency for the low-momentum pion from the D^{*-} decay, since it is highly correlated with the D^{*-} momentum and thereby with w. The functions parametrizing the efficiency for data and MC simulation are consistent within the statistical uncertainties. To assess the systematic uncertainty on $|V_{cb}|$, we vary the parameters of the efficiency function by their uncertainty, including correlations. We add in quadrature the uncertainty in the absolute scale as determined from higher-momentum tracks reconstructed in both the SVT and the DCH. The resulting systematic uncertainty on $|V_{cb}|$ is 1.3%.

3. D^*l vertex reconstruction efficiency

The uncertainties from the D^*l vertex reconstruction have been evaluated by observing the impact of changes

TABLE III. Results of fits performed separately for the six subsamples corresponding to each combination of three $\bar{D}^0$ decay modes and the charged lepton. The uncertainties represent the total uncertainty of the fit, except for $\mathcal{F}(1)|V_{cb}|$, where it is split into the statistical and the systematic contribution included in the fit.

Subsample	ρ^2	$R_1(1)$	$R_2(1)$	$\mathcal{F}(1)\|V_{cb}\| \times 10^3$	χ^2/d.o.f.
$K\pi e$	0.971 ± 0.163	1.166 ± 0.182	0.977 ± 0.107	$34.76 \pm 0.61 \pm 0.61$	23.9/24
$K\pi\mu$	1.013 ± 0.175	1.193 ± 0.206	0.922 ± 0.123	$34.55 \pm 0.66 \pm 0.65$	37.9/24
$K\pi\pi\pi e$	1.581 ± 0.151	2.043 ± 0.384	0.405 ± 0.232	$33.30 \pm 1.27 \pm 0.96$	15.6/24
$K\pi\pi\pi\mu$	1.146 ± 0.258	1.156 ± 0.351	0.946 ± 0.197	$34.14 \pm 1.10 \pm 0.98$	28.0/24
$K\pi\pi^0 e$	1.042 ± 0.165	1.217 ± 0.206	0.926 ± 0.118	$34.86 \pm 0.64 \pm 1.46$	26.9/24
$K\pi\pi^0\mu$	1.170 ± 0.155	1.439 ± 0.228	0.838 ± 0.131	$34.38 \pm 0.74 \pm 1.46$	24.8/24

TABLE IV. Breakdown of statistical and systematic uncertainties.

	ρ^2	$R_1(1)$	$R_2(1)$	$\mathcal{F}(1)\lvert V_{cb}\rvert \times 10^3$	$\mathcal{B}(B^0 \to D^{*-}\ell^+\nu_\ell) \times 10^2$
Statistical error	0.094	0.131	0.077	0.41	0.05
PID, tracking, $\mathcal{B}(D^0)$	0.003	0.006	0.002	0.75	0.21
Soft-π efficiency	0.013	0.005	0.001	0.46	0.18
$D^* l$ vertex fit	0.014	0.010	0.008	0.06	0.06
B-momentum variation	0.013	0.040	0.017	0.29	0.14
Radiative corrections	0.005	0.004	0.000	0.19	0.07
D^{**} composition	0.011	0.008	0.009	0.10	0.07
Background estimates	0.006	0.004	0.002	0.04	0.04
Partial systematic error	0.027	0.043	0.021	0.95	0.33
B^0 lifetime	...	...	...	0.10	0.03
$B\bar{B}$ normalization	...	...	...	0.19	0.05
$\mathcal{B}(D^* \to D^0\pi)$	...	...	...	0.13	0.04
f_{+-}/f_{00}	0.003	0.003	0.002	0.25	0.07
Total systematic error	0.027	0.043	0.021	1.01	0.34

in the standard vertex fit procedure. First, we remove the constraint on the average position of the beam-beam interaction point, and second, we remove the lepton track from the vertex fit. We take the larger of the observed variations of the parameters as the systematic uncertainty.

4. B momentum

The B momentum is impacted by small changes in the energies of the two colliding beams. In the Monte Carlo simulation the beam energies are assumed to be constant. We have examined the impact of these variations on the measured distributions and have concluded that we can account for this difference by rescaling the $\cos\theta_{B,D^*\ell}$ values in the simulation by a factor of 0.97. Half of the observed relative change of the fitted parameters coming from the adjustment is assumed as the systematic uncertainty due to this effect. This is the largest systematic uncertainty on $R_1(1)$ and $R_2(1)$.

5. Radiative corrections

Radiative corrections to the $B^0 \to D^{*-}\ell^+\nu_\ell$ decays are simulated by PHOTOS 2.0 [23], which describes the final state photon radiation (FSR) up to $\mathcal{O}(\alpha^2)$. In the event reconstruction, no attempt is made to recover photons emitted in the decay. The simulated prediction of the reconstructed kinematic variables is sensitive to the details of the radiative corrections. This is particularly important for electrons, for which FSR results in the long tail below -1 in the $\cos\theta_{B,D^*\ell}$ distribution.

At present, no detailed calculation of the full $\mathcal{O}(\alpha)$ radiative corrections to the $B^0 \to D^{*-}\ell^+\nu_\ell$ decay is available. Recently, a new $\mathcal{O}(\alpha)$ calculation of radiative corrections in $K^0 \to \pi^- e^+ \nu_e$ decays has become available [28], which allows detailed comparisons of the radiated photons with data and with PHOTOS calculations. These new calculations agree well with kaon data. From the comparison with PHOTOS, it is evident that the radiated photon energy spectrum is reproduced quite well by PHOTOS, but the photon emission angle with respect to the electron differs significantly.

To assess the systematic uncertainty due to the imperfect treatment of the radiative corrections in B decays, we have used the comparison presented in Ref. [28] and reweighted the simulated decays to reproduce the photon angular distribution for photons above 10 MeV in the B rest frame. The effect of the reweighting has been used as an estimate of the systematic uncertainty. The possible impact of the radiative effects on the hadronic interactions, i.e. the form factors, is unknown and therefore not considered.

6. $B \to D^* X \ell \nu_\ell$ background description

The semileptonic branching fraction and form factors for the four higher-mass charm states, D^{**}, and for nonresonant production of $D\pi$ and $D^*\pi$ are not well known. The shapes of these different components of the $B \to D^* X \ell \nu_\ell$ background are taken from simulation. Their relative yield is obtained from the fit to the $\cos\theta_{B,D^*\ell}$ distribution. To account for the uncertainty of the composition of this background, the fits have been repeated using only one of the contributions at a time. The study was done only for the $\bar{D}^0 \to K^+\pi^-$ subsample; it is assumed to be valid also for the other subsamples. The estimated uncertainty on the fit parameters is taken as half of the biggest change observed.

7. Background estimates

As explained in Sec. V B the background covariance matrix is built using the measured background shape in one observable, and the simulation information for the

others. The choice of the observable is arbitrary. The systematic uncertainty is evaluated by comparing results for the four kinematic observables. The maximum observed variation with respect to the standard fit result is taken as the estimate for this uncertainty.

8. Global normalization factors

There are several quantities that affect only the overall normalization of the data, and thus not the form-factor parameters. Their contributions to the systematic uncertainty on $\mathcal{F}(1)|V_{cb}|$ and the branching fraction are listed in the bottom half of Table IV. They are as follows: the B^0 lifetime $\tau_{B^0} = 1.530 \pm 0.009$ [13], the $D^{*-} \to \bar{D}^0\pi^-$ branching fraction $\mathcal{B}(D^{*-} \to \bar{D}^0\pi^-) = 67.7 \pm 0.5\%$, and $N_{B\bar{B}}$, the number of $B\bar{B}$ events in the total data sample. The systematic uncertainty on $N_{B\bar{B}}$ is 1.1%.

The effect of the uncertainties in the $\bar{D}^0$ branching fractions has already been discussed; it is subsample specific, but it affects all parameters because it changes the fraction of signal events from different $\bar{D}^0$ decays.

The uncertainty on the ratio $f_{+-}/f_{00} = \mathcal{B}(\Upsilon(4S) \to B^+B^-)/\mathcal{B}(\Upsilon(4S) \to B^0\bar{B}^0) = 1.037 \pm 0.029$ [13] affects both the absolute number of measured $B^0 \to D^{*-}\ell^+\nu_\ell$ decays and the ratio of background events from B^0 and $B^\pm$ decays in the simulation. This second aspect influences the $\cos\theta_{B,D^*\ell}$ distributions and therefore the background determination. For this reason, this uncertainty also affects the form-factor parameters. The systematic uncertainty is equated with the observed change in the fit parameters for a 1 standard deviation change in the value of f_{+-}/f_{00}.

VII. CONCLUSIONS

A. Summary of results of this analysis

A sample of about 52 800 fully reconstructed $B^0 \to D^{*-}\ell^+\nu_\ell$ decays recorded by the *BABAR* detector has been analyzed to extract both $\mathcal{F}(1)|V_{cb}|$ and the form-factor parameters, ρ^2, $R_1(1)$, and $R_2(1)$, in the Caprini-Lellouch-Neubert parametrization [18]. The D^{*-} candidates are reconstructed from the $D^{*-} \to \bar{D}^0\pi^-$ decays, and the $\bar{D}^0$ mesons are reconstructed in three different decay modes, $K^+\pi^-$, $K^+\pi^-\pi^+\pi^-$, and $K^+\pi^-\pi^0$. Electrons or muons are paired with the D^{*-} to form signal candidates. The large data sample has permitted a more precise determination of the background contributions, largely based on data, and thus has resulted in smaller experimental uncertainties.

The results of the simultaneous fit to three one-dimensional projections of the decay rate are

$$\begin{aligned}\mathcal{F}(1)|V_{cb}| &= (34.7 \pm 0.4 \pm 1.0) \times 10^{-3},\\ \rho^2 &= 1.157 \pm 0.094 \pm 0.027,\\ R_1(1) &= 1.327 \pm 0.131 \pm 0.043,\\ R_2(1) &= 0.859 \pm 0.077 \pm 0.021.\end{aligned}$$

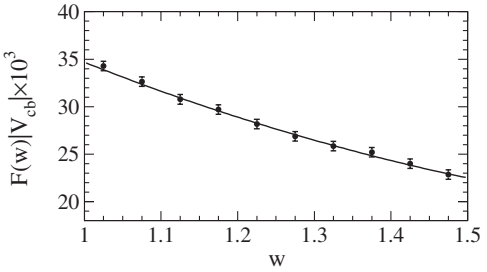

FIG. 6. The measured w dependence of $\mathcal{F}(w)|V_{cb}|$ (data points) compared to the theoretical function with the fitted parameters (solid line). The experimental uncertainties are too small to be visible.

The stated uncertainties of the measurement here are the statistical and the total systematic one. The simultaneous fit to the three distributions reduces the uncertainty due to the form-factor parameters.

Using an unquenched lattice calculation giving $\mathcal{F}(1) = 0.919^{+0.030}_{-0.035}$ [15] results in the following value for $|V_{cb}|$,

$$|V_{cb}| = (37.8 \pm 0.4 \pm 1.1^{+1.2}_{-1.4}) \times 10^{-3}.$$

Here the third error is due to the theoretical uncertainty in $\mathcal{F}(1)$. Figure 6 shows the measured decay rate, integrated over angles, $\mathcal{F}(w)|V_{cb}|$, as well as the fitted theoretical w dependence [see Eq. (11)].

The branching fraction for the decay $B^0 \to D^{*-}\ell^+\nu_\ell$ is

$$\mathcal{B}(B^0 \to D^{*-}\ell^+\nu_\ell) = (4.72 \pm 0.05 \pm 0.34)\%.$$

B. Combination of results with the previous *BABAR* measurement of the form-factor parameters

The *BABAR* Collaboration recently published a measurement [12] of the same form-factor parameters for $B^0 \to D^{*-}\ell^+\nu_\ell$ decays based on an unbinned maximum-likelihood fit to the four-dimensional decay distribution [Eq. (10)]. This fit is sensitive to the interference of the three helicity amplitudes and thus results in significant smaller uncertainties on the form-factor parameters. The fit does not attempt an absolute normalization of the decays, and thus is not sensitive to $\mathcal{F}(1)|V_{cb}|$. It resulted in $\rho^2 = 1.145 \pm 0.066 \pm 0.035$, $R_1(1) = 1.396 \pm 0.070 \pm 0.027$, and $R_2(1) = 0.885 \pm 0.046 \pm 0.013$.

We combine the two *BABAR* measurements of the form-factor parameters, taking into account the correlation between them, and obtain

$$\begin{aligned}\mathcal{F}(1)|V_{cb}| &= (34.4 \pm 0.3 \pm 1.1) \times 10^{-3},\\ \rho^2 &= 1.191 \pm 0.048 \pm 0.028,\\ R_1(1) &= 1.429 \pm 0.061 \pm 0.044,\\ R_2(1) &= 0.827 \pm 0.038 \pm 0.022.\end{aligned}$$

Compared to the analysis presented in this paper, the combined result has significantly smaller statistical uncer-

tainties of the form-factor parameters. The event sample and the sample of Monte Carlo simulated events used in Ref. [12] are a subset of the one used in the present analysis, namely, about 15 000 selected $\bar{B}^0$ candidates with $\bar{D}^0 \to K^+\pi^-$ decays combined with electrons. Except for the selection of the $\bar{D}^0$ decay, the event selection and the determination of the background shapes and the signal extraction are almost identical for the two analyses. Therefore, all the detector-related systematic uncertainties should be the same, as well as the uncertainties from the background models and those due to input parameters as the branching fractions. Thus, we retain the systematic measurement uncertainties established in this paper. The combined statistical errors are still larger than the total systematic uncertainties, but not by a large factor. An upper limit for the correlation between the two measurements has been estimated on the basis of the ratio of the uncertainties, and is found to be less than 0.45.

The correlation coefficients for the combined measurements are

$$\begin{aligned}
\rho(\rho^2, R_1(1)) &= +71\%, \\
\rho(\rho^2, R_2(1)) &= -83\%, \\
\rho(\rho^2, \mathcal{F}(1)|V_{cb}|) &= +27\%, \\
\rho(R_1(1), R_2(1)) &= -84\%, \\
\rho(R_1(1), \mathcal{F}(1)|V_{cb}|) &= -39\%, \\
\rho(R_2(1), \mathcal{F}(1)|V_{cb}|) &= +22\%.
\end{aligned}$$

Figure 7 shows the correlations between the fitted variables and their uncertainties, both for the present analysis and for the combined result with Ref. [12]. The contours correspond to $\Delta\chi^2 = 1$, i.e. 39% CL. The correlations between the form-factor parameters are quite large, but their correlation with $\mathcal{F}(1)|V_{cb}|$ is less than 0.4, and the sign of the coefficients differs, resulting in a much reduced overall dependence of $\mathcal{F}(1)|V_{cb}|$ on these form factors.

Using the same lattice calculation for $\mathcal{F}(1)$ [15], we obtain an improved value for $|V_{cb}|$,

$$|V_{cb}| = (37.4 \pm 0.3 \pm 1.2^{+1.2}_{-1.4}) \times 10^{-3},$$

where the third error reflects the current uncertainty on $\mathcal{F}(1)$.

The corresponding branching fraction of the decay $B^0 \to D^{*-}\ell^+\nu_\ell$ is

$$\mathcal{B}(B^0 \to D^{*-}\ell^+\nu_\ell) = (4.69 \pm 0.04 \pm 0.34)\%.$$

The combined results of the two *BABAR* analyses supersede all previous *BABAR* measurements of the form-factor parameters, of the exclusive branching fraction for the $B^0 \to D^{*-}\ell^+\nu_\ell$ decay, and of $|V_{cb}|$ extracted from this decay.

The value of the branching fraction presented here is smaller than the average of previous measurements [13]. This measurement combined with $\mathcal{B}(B^0 \to D^-\ell\nu_\ell) = (2.08 \pm 0.18)\%$ [13] represents only $(65 \pm 7)\%$ of the total branching fraction for the $B^0 \to X_c\ell\nu_\ell$ decays. The remaining fraction of 35% is expected to involve higher-mass charm states. The branching fractions for decays to

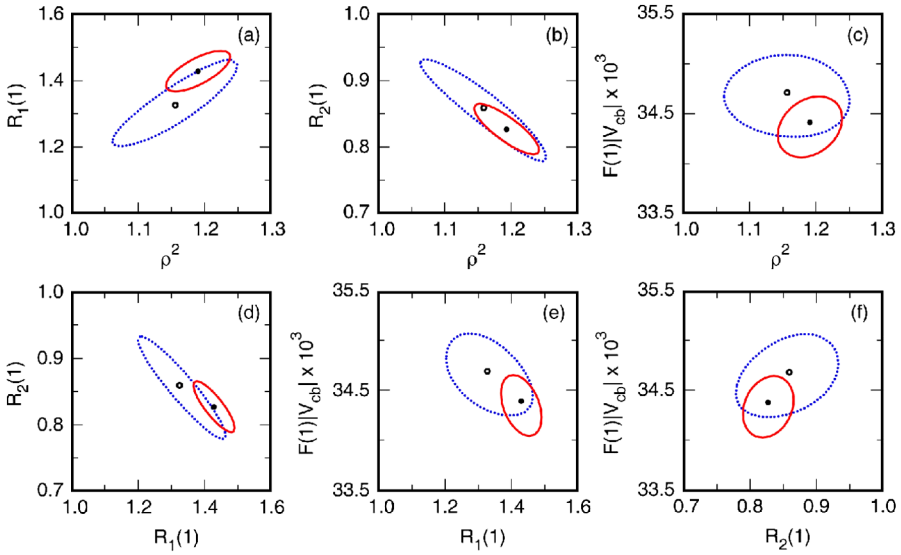

FIG. 7 (color online). Correlations between fitted variables and their uncertainties, both for the present analysis with the statistical uncertainties (dotted line, central value marked with an open circle) and for the combined result with the total experimental uncertainties, i.e. the statistical and systematic uncertainties combined (solid line, central value marked with a solid dot): (a) $\rho^2 - R_1(1)$, (b) $\rho^2 - R_2(1)$, (c) $\rho^2 - \mathcal{F}(1)|V_{cb}| \times 10^3$, (d) $R_1(1) - R_2(1)$, (e) $\mathcal{R}_1(1) - \mathcal{F}(1)|V_{cb}| \times 10^3$, and (f) $R_2(1) - \mathcal{F}(1)|V_{cb}| \times 10^3$ projections. The contours correspond to $\Delta\chi^2 = 1$, i.e. 39% CL.

these individual higher-mass states are not well known, in particular, those involving broad resonances or nonresonant $D^{(*,**)}\pi$ states [29,30].

The combination of the two *BABAR* measurements results in a further reduction of the form-factor uncertainties compared to the previous *BABAR* analysis [12], for which the uncertainties on $R_1(1)$ and $R_2(1)$ had already been reduced by a factor of 4 or more, compared to the CLEO measurement [11]. The uncertainty on ρ^2 has also been reduced, by a factor of 5 with respect to the *BABAR* measurement in Ref. [10]. The correlation between $\mathcal{F}(1)|V_{cb}|$ and ρ^2, which was sizable for all previous measurements, has been reduced significantly, and this also leads to a smaller uncertainty for $|V_{cb}|$.

The resulting value of $|V_{cb}|$ is fully compatible with the earlier *BABAR* measurement [10], and most earlier measurements [13], but it is significantly smaller than the CLEO measurement [31].

$|V_{cb}|$ can also be extracted from inclusive $B \to X_c \ell \nu_\ell$ decays. Recent measurements of $|V_{cb}|$ rely on moments of the electron energy and the hadron mass spectrum, combined with moments of the energy photon spectrum in inclusive $B \to X_s \gamma$ decays. Here X_c and X_s refer to charm and strange hadronic states, resonant or nonresonant. Global fits to such moments, as a function of the minimum lepton and photon energy, have been performed in terms of two different QCD calculations, one in the so-called 1S scheme [32] and the other in the kinetic scheme [33]. The results are in very good agreement. The weighted average is $|V_{cb}| = (41.7 \pm 0.7) \times 10^{-3}$ [13]; the experimental and theoretical uncertainties are comparable in size. The experimental techniques and the theoretical calculations for exclusive and inclusive decays are completely different and uncorrelated. Given the sizable experimental error and the large uncertainty of the form-factor normalization of the exclusive measurement, the results are consistent. This should give us confidence in the experimental methods employed and the theoretical calculations, but also an incentive to improve on both.

ACKNOWLEDGMENTS

We are grateful for the extraordinary contributions of our PEP-II colleagues in achieving the excellent luminosity and machine conditions that have made this work possible. The success of this project also relies critically on the expertise and dedication of the computing organizations that support *BABAR*. The collaborating institutions wish to thank SLAC for its support and the kind hospitality extended to them. This work is supported by the U.S. Department of Energy and National Science Foundation, the Natural Sciences and Engineering Research Council (Canada), the Commissariat à l'Energie Atomique and Institut National de Physique Nucléaire et de Physique des Particules (France), the Bundesministerium für Bildung und Forschung and Deutsche Forschungsgemeinschaft (Germany), the Istituto Nazionale di Fisica Nucleare (Italy), the Foundation for Fundamental Research on Matter (The Netherlands), the Research Council of Norway, the Ministry of Science and Technology of the Russian Federation, Ministerio de Educación y Ciencia (Spain), and the Particle Physics and Astronomy Research Council (United Kingdom). Individuals have received support from the Marie-Curie IEF program (European Union) and the A. P. Sloan Foundation.

[1] Charge conjugate decay modes are implicitly included, and ℓ refers to a charged lepton, either an electron or muon.
[2] M. Neubert, Phys. Rep. **245**, 259 (1994).
[3] J. D. Richman and P. R. Burchat, Rev. Mod. Phys. **67**, 893 (1995).
[4] H. Albrecht *et al.* (ARGUS Collaboration), Z. Phys. C **57**, 533 (1993).
[5] K. Abe *et al.* (Belle Collaboration), Phys. Lett. B **526**, 247 (2002).
[6] B. Buskulic *et al.* (ALEPH Collaboration), Phys. Lett. B **359**, 236 (1995).
[7] B. Buskulic *et al.* (ALEPH Collaboration), Phys. Lett. B **395**, 373 (1997).
[8] K. Ackerstaff *et al.* (OPAL Collaboration), Phys. Lett. B **395**, 128 (1997).
[9] P. Abreu *et al.* (DELPHI Collaboration), Phys. Lett. B **510**, 55 (2001).
[10] B. Aubert *et al.* (*BABAR* Collaboration), Phys. Rev. D **71**, 051502 (2005).
[11] J. E. Duboscq *et al.* (CLEO Collaboration), Phys. Rev. Lett. **76**, 3898 (1996).
[12] B. Aubert *et al.* (*BABAR* Collaboration), Phys. Rev. D **74**, 092004 (2006).
[13] W. M. Yao *et al.* (Particle Data Group), J. Phys. G **33**, 1 (2006), 2007 partial update for edition 2008.
[14] N. Isgur and M. B. Wise, Phys. Lett. B **232**, 113 (1989); **237**, 527 (1990).
[15] S. Hashimoto *et al.*, Phys. Rev. D **66**, 014503 (2002).
[16] N. G. Uraltsev, in *At the Frontier of Particle Physics: Handbook of QCD* (World Scientific, Singapore, 2001).
[17] A. Czarnecki and K. Melnikov, Nucl. Phys. **B505**, 65 (1997).
[18] I. Caprini, L. Lellouch, and M. Neubert, Nucl. Phys. **B530**, 153 (1998).
[19] B. Aubert *et al.* (*BABAR* Collaboration), Nucl. Instrum. Methods Phys. Res., Sect. A **479**, 1 (2002).
[20] B. Aubert *et al.* (*BABAR* Collaboration), Phys. Rev. D **66**,

032003 (2002).
[21] B. Aubert *et al.* (*BABAR* Collaboration), Phys. Rev. D **67**, 031101 (2003).
[22] S. Agostinelli *et al.* (Geant4 Collaboration), Nucl. Instrum. Methods Phys. Res., Sect. A **506**, 250 (2003).
[23] E. Barberio and Z. Was, Comput. Phys. Commun. **79**, 291 (1994).
[24] D. Scora and N. Isgur, Phys. Rev. D **52**, 2783 (1995).
[25] J. L. Goity and W. Roberts, Phys. Rev. D **51**, 3459 (1995).
[26] P. L. Fabretti *et al.* (E687 Collaboration), Phys. Lett. B **331**, 217 (1994).
[27] F. James, ''MINUIT: Function Minimization and Error Analysis,'' CERN Program Library Long Writeup D506.
[28] T. Andre, Ann. Phys. (N.Y.) **322**, 2518 (2007); J. Phys. G **33**, 1 (2006).
[29] K. Liventsev *et al.* (Belle Collaboration), Phys. Rev. D **72**, 051109 (2005).
[30] B. Aubert *et al.* (*BABAR* Collaboration), Phys. Rev. D **76**, 051101 (2007)
[31] N. E. Adam *et al.* (CLEO Collaboration), Phys. Rev. D **67**, 032001 (2003).
[32] C. W. Bauer *et al.*, Phys. Rev. D **70**, 094017 (2004).
[33] O. Buchmüller and H. Flächer, Phys. Rev. D **73**, 073008 (2006).